Defect levels of carbon-related defects at the SiC/SiO_2 interface from hybrid functionals

Fabien Devynck, Audrius Alkauskas, Peter Broqvist, and Alfredo Pasquarello

Chaire de Simulation à l'Echelle Atomique (CSEA), Ecole Polytechnique Fédérale de Lausanne (EPFL), CH-1015 Lausanne, Switzerland

(Received 8 December 2010; revised manuscript received 8 April 2011; published 16 May 2011)

We investigate carbon single-atom and pair defects at the SiC/SiO_2 interface as candidate defects for the density of defect states in the SiC band gap. In order to accurately describe the electronic defect levels with respect to the SiC band edges, we use a hybrid density functional which reproduces the experimental band gap of SiC. The carbon pair defect consisting of two neighboring sp^2 hybridized carbon atoms is modeled in various configurations within a SiC/SiO_2 model interface showing good structural parameters and an oxide density typical of amorphous SiO_2. The carbon pair defect is found to contribute to the density of defect states not only in the lower and/or mid band gap of SiC, but also in the upper band gap, in contrast with previous studies. The carbonpair defect is also investigated via molecular models to achieve insight into the energy range spanned by its defect levels when the relative orientation of its sp^2 hybridization planes and the chemical nature of its neighbors are varied. Carbon single-atom defects on the oxide side of the interface are also modeled and found to contribute to the defect density in the band gap in a similar way as carbonpair defects. Comparison to the experimental defect density suggests that defects involving one or two carbon atoms cannot account for the high defect density observed in the vicinity of the SiC conduction band.

DOI: 10.1103/PhysRevB.83.195319 PACS number(s): 68.35.Ct, 73.20.−r, 71.15.Pd

I. INTRODUCTION

With its high band gap and its thermal oxide SiO_2, silicon carbide (SiC) is the candidate of choice for high power metal-oxide-semiconductor devices. However, in contrast with the Si/SiO_2 interface, the SiC/SiO_2 interface features a high density of defect states (D_{it}) reaching 10^{13} cm^{-2} eV^{-1} near the 4H-SiC conduction band, which hinders its use in the semiconductor industry. The high D_{it} is generally attributed to carbon-related defects.[1–3] Indeed, a systematically higher D_{it} is observed on oxidized SiC faces composed of a higher density of carbon atoms.[2] The preoxidation cleaning of SiC surfaces by exposing them to ultraviolet radiation and oxygen was shown to result in a significant improvement in the electronic properties of SiC/SiO_2 interfaces. It was proposed that the surface defects that are removed by oxidation are probably carbon clusters.[1] Based on a comparison between the internal photoemission spectra of SiC/SiO_2 interfaces and of hydrogenated amorphous carbon films deposited on SiO_2, it was suggested that the formation of π-bonded carbon clusters of different sizes could account for a quasicontinuum spectrum of interface states throughout the SiC band gap, the size of the clusters determining the position of the upper filled electron states, and the π–π^* splitting.[2,4] Graphitic arrangements were observed at the unoxidized SiC surfaces, but such structures could not be detected by x-ray photoelectron spectroscopy after *in situ* oxidation.[5,6] Even if the presence of large graphitic clusters at the SiC/SiO_2 interface could not be firmly established, smaller size clusters or individual carbon-related defects could occur as by-products of the oxidation. More recently, electron paramagnetic resonance (EPR) experiments on oxidized porous SiC identified carbon dangling bonds.[7] These defects could successfully be passivated by H_2 at 400 °C,[8] but it remains unclear to which fraction of the electrically active interface defects these observations pertain. Recently, it was shown that a postoxidation anneal in nitric oxide followed by a postmetallization anneal in hydrogen through a platinum gate known to catalyze atomic hydrogen formation resulted in a reduction of the trap density by over an order of magnitude near the conduction band.[9,10] It was suggested that this treatment could eliminate the threefold coordinated atoms responsible for the high interface trap density either by hydrogen passivation or by nitrogen replacement.[10,11]

Recent density-functional calculations shed some light on both the atomic-scale oxidation mechanism of 4H-SiC and the nature of possible defects at the SiC/SiO_2 interface.[11–14] Knaup *et al.* first studied typical defects occurring on the semiconductor side of the interface and identified carbon-related defects corresponding to the D_{it} in the lower part of the SiC band gap.[12] The same authors then focused on the oxide side of the interface, identifying Si interstitials and doubly bonded C–C dimers as candidate defects with energy levels close to the SiC conduction band.[11,13] In a subsequent study, Wang *et al.* considered correlated carbon dangling bonds as a possible origin for the D_{it} in the SiC band gap.[14]

Density-functional calculations are indeed a powerful tool to investigate the nature of defects at the SiC/SiO_2 interface. However, the determination of defect levels faces the difficulty that the common local and semilocal density-functional approaches fail in giving a good description of the band gap. Furthermore, another difficulty consists of the realistic modeling of the interface as the electronic properties of the defect levels depend on the local environment.

In this work, we study a variety of carbon single-atom and pair defects located in the vicinity of the SiC–SiO_2 interface. We make use of an atomistic model of the interface showing good structural parameters and an oxide density typical of amorphous SiO_2.[15] To overcome the band gap limitations of local and semilocal density-functional schemes, we adopt a hybrid density functional[16] which gives a band gap for SiC matching the experimental one. For each considered defect configuration, our study thus gives the corresponding defect levels within the SiC band gap. These results provide a basis toward the interpretation of the experimental density of defect states at the SiC–SiO_2 interface.

The present paper is organized as follows. Section II is devoted to the description of the methods and of the atomistic models used in this work. In Sec. III, we consider carbon pair defects in various configurations, both in the substrate and in the oxide, and discuss the position of their calculated energy levels. The C–C pair defect is then examined through a systematic study of molecular models. Single-atom carbon defects in the oxide are also considered. The conclusions are drawn in Sec. IV.

II. METHODS AND MODELS

The electronic structure is described within a spin-polarized density-functional scheme, in which the exchange-correlation energy is given by the generalized gradient approximation proposed by Perdew, Burke, and Ernzerhof (PBE).[17] For the wave functions of the valence electrons, we use a plane-wave basis set with a cutoff energy of 70 Ry. In all calculations, core-valence interactions are described by norm-conserving PBE pseudopotentials.[18] All models undergo full structural relaxations at the PBE level. To achieve an improved description of the SiC band gap, we then address the electronic properties using hybrid PBE density functionals,[16] in which a fraction of the PBE exchange interaction is replaced by nonlocal Fock exchange. Following a recently proposed approach,[19] the fraction of Fock exchange included in the calculations is tuned to recover the experimental band gap of SiC. For notation convenience, the fraction α of included Fock exchange will be denoted in parentheses after the functional acronym, that is, PBE(α). We take care of the integrable divergence of the exchange term, thus enabling Γ-point sampling.[20] We here use the CPMD package.[21]

The description of the SiC band gap is essential for an accurate representation and positioning of the defect levels. We consider in this work both 4H-SiC and 6H-SiC substrates. For reference, we first study these substrates in their bulk phase, that is, crystalline 4H-SiC and 6H-SiC. We model hexagonal 4H-SiC and 6H-SiC using a 96-atom structure and a 144-atom structure, respectively. The experimental values of 3.2714 and 4.9073 for the c/a ratio are used for 4H-SiC and 6H-SiC, respectively.[22] With the PBE functional, we find an equilibrium lattice constant a of 3.096 Å for both SiC polytypes, in excellent agreement with the experimental values of 3.073 and 3.081 Å for 4H-SiC and 6H-SiC, respectively. The 4H-SiC and 6H-SiC band gaps calculated at the PBE level (2.2 and 2.0 eV, respectively) severely underestimate the experimental values (3.3 and 3.0 eV; Ref. 22), as usual at this level of theory. This limitation is overcome by the use of a hybrid density functional including 15% of nonlocal Fock exchange. When aligning the electrostatic potential, we find the valence band edge shifting down by $\sim$0.6 eV and the conduction band edge shifting up by $\sim$0.4 eV. Thus, the fraction of 15% Fock exchange yields band gaps in close agreement with the experimental ones for both SiC polytypes.

The 4H-SiC/SiO_2 model interface used here was generated previously through a sequential scheme involving classical molecular dynamics and density functional calculations.[15] Our model contains a crystalline substrate with 8 planes of alternating Si and C atoms (8.2 Å thick) connected without any coordination defect to an amorphous oxide layer with a thickness of 16 Å. The model structure shows good structural parameters and an oxide density typical of amorphous SiO_2.[15] The 6H-SiC/SiO_2 model interface was then generated by substituting the 8-plane 4H-SiC substrate with a 12-plane 6H-SiC substrate and allowing the structure to relax further.

Via the use of a hybrid functional with a fixed fraction of Fock exchange it is not possible to recover the experimental band gaps for both interface components. Indeed, the use of $\alpha = 0.15$ required for SiC is inappropriate for the band gap of SiO_2, which is reproduced with $\alpha = 0.35$.[19] Since it is important to situate the defect levels with respect to the SiC band edges, our priority is to ensure an accurate description of the SiC band gap. The calculations involving the interface model are therefore carried out with $\alpha = 0.15$. Furthermore, we note that the interface calculations are subject to the quantum confinement effect due to the finite thickness of the SiC slab. This effect leads to a spurious increase of the SiC band gap in the interface calculation. To address this effect, the proper position of the SiC band edges are determined in a defect-free bulk model of SiC and reported with respect to the electronic structure of the interface calculation through the alignment of the electrostatic potential.

The defects selected in the present work have been identified as possible products occurring during the SiC oxidation process.[11–14] In the present work, we refrain from giving defect formation energies because of the amorphous SiO_2 component in our model. Indeed, the determination of defect formation energies is delicate for such models, because it is difficult to distinguish defect-induced relaxations from lattice relaxations.[23]

The defect states in this work are studied through their (generalized) Kohn-Sham energy levels. This representation emphasizes chemical intuition through a picture based on molecular orbitals. In the specific case of defect levels at SiC/SiO_2 interfaces, a description in terms of Kohn-Sham levels also offers a straightforward comparison with previous studies.[11–14] Furthermore, the Kohn-Sham levels are generally found to be in good agreement with vertical charge transition levels. Such levels are found by considering a charge transition without allowing the system to undergo structural relaxation. However, the use of the Kohn-Sham spectrum for the determination of defect levels does not account for structural relaxation effects that could occur upon charging. For specific defects, these effects have been found to be negligible when evaluated with a screened hybrid functional,[24] but this result cannot trivially be generalized to any kind of defect system. Such effects could in principle be determined through the calculation of thermodynamic charge transition levels involving total-energy differences between structurally relaxed defect states of different charge. However, the treatment of charged defects in periodic systems suffers from sizable finite-size effects, for which a reliable correction scheme in the case of defects at interfaces is not yet available. For illustration, we provide below an estimate of the difference between Kohn-Sham and charge transition levels for one bulk defect of the same kind as those studied at the interface.

In following, the defect levels are given within a band diagram pertaining to the 4H-SiC polytype, which shows the largest band gap among the two polytypes. In case the defects

need to be referred to the band edges of 6H-SiC, these can be found by lowering the SiC conduction band edge by 0.3 eV.

III. DEFECT LEVELS OF CARBON-RELATED DEFECTS

Conventional oxidation of SiC results in a much higher defect density of states at SiC/SiO_2 interfaces than at Si/SiO_2 interfaces. The most obvious difference in the oxidation of the two semiconductors is that the key atomic-scale oxidation step of SiC entails carbon release. The incomplete removal of carbon could lead to various forms of carbon-related defects in either the near interface SiC substrate or SiO_2 oxide. We start our study of carbon-related defects with the most simple one, that is, the single-carbon interstitial.

A. Single-carbon interstitial in bulk SiC

Despite the neglect of interface specific effects, a bulk model of SiC provides an adequate starting point for describing the main features of the single-carbon interstitial. We use the 96-atom model of bulk 4H-SiC described in Sec. II and introduce an extra carbon atom at a C lattice site, as shown in Fig. 1. Upon full relaxation, one notices that structural adjustments mainly occur in the immediate vicinity of the two neighbor carbon atoms. The volume of the tetrahedron defined by the four silicon atoms enclosing the C–C pair increases by 10% upon insertion of the additional carbon atom. With a value of 1.79 Å, the average Si–C distance involving one C atom of the pair decreases by 6% compared to bulk SiC. The average Si–C–Si angle is 138.4° (±1.4°) and the C–C bond is 1.37 Å. Finally, the angle between the planes of the two sp^2 hybridized carbon atoms is 89.3°, and the average dihedral angle Si–C–C–Si involving the C–C pair is 85.3° (with a standard deviation of 2.1°).

We then study the electronic structure of the carbon interstitial defect using a spin-polarized density-functional approach at the PBE and PBE(0.15) levels of theory.[16,17] The defect levels are aligned to the band edges of the defect-free bulk model of 4H-SiC through the local electrostatic potential. At a distance greater than 3 Å from the carbon interstitial, the local electrostatic potential is unaffected by the defect. The energy differences between the average electrostatic potential and the band edges are therefore determined in the defect-free bulk model of 4H-SiC and reported with respect to the local

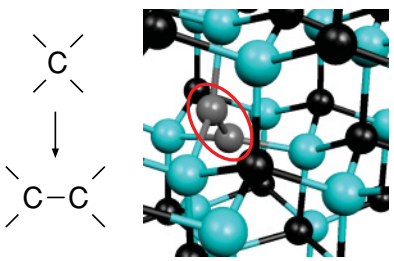

FIG. 1. (Color online) Carbon interstitial at a carbon site in a bulk model of 4H-SiC. The ellipse circles the resulting two sp^2 hybridized carbon atoms represented in dark gray. Fourfold coordinated carbon and silicon atoms are represented in black and light gray (cyan), respectively. The schematics illustrates the bonding configuration before and after the defect creation.

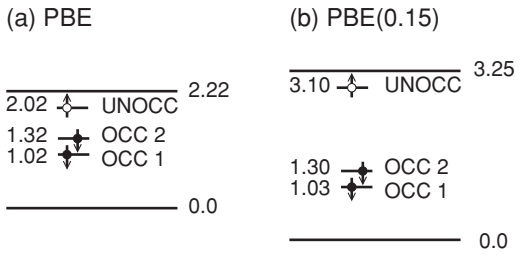

FIG. 2. C–C pair-related defect levels in the 4H-SiC band gap, calculated with the PBE and PBE(0.15) functionals in bulk 4H-SiC. The majority and minority spin electrons are denoted by downward and upward arrows, respectively, and the occupied and unoccupied levels are represented by solid and open circles, respectively. The valence band maximum is taken as the origin. Energies are given in eV.

electrostatic potential far from the carbon interstitial in the defect model to retrieve the correct positions of the band edges. Figure 2 shows three defect levels located in the band gap of SiC, in both the PBE and the PBE(0.15) calculations. Two levels, located at or below midgap in the PBE and PBE(0.15) calculations, respectively, are occupied, while one defect located just below the conduction band is unoccupied. When comparing the description of the defect levels in the PBE and PBE(0.15) calculations, one observes a very good agreement for the positions of the occupied levels with respect to the valence band edge. Similarly, a very good agreement for the unoccupied level is observed when referred to the conduction band. The two occupied levels are located at ∼1.0 and ∼1.3 eV above the valence band while the unoccupied level is ∼0.2 eV below the conduction band. In the hybrid functional calculation, the valence band shifts down with respect to the local electrostatic potential, while the conduction band moves up (cf. Sec. II). Upon the inclusion of a fraction of nonlocal Fock exchange, the occupied and unoccupied defect levels are therefore affected in a similar manner as the valence and conduction bands, respectively.

The projections of the states in the SiC band gap on the atomic orbitals allow one to identify the carbon atoms of the C–C pair as the origin of the defect states. The isosurfaces of the density (viz. the square of the wave function) of the three defect states are plotted in Fig. 3. The C–C pair is composed of two sp^2 hybridized carbon atoms. However, the planes of their sp^2 orbitals are nearly perpendicular, which results in a single σ bond with an energy level located below the valence band maximum. Two singly occupied p orbitals (one on each carbon atom) account for the occupied levels in the band gap [Figs. 3(a) and 3(b)]. Their corresponding unoccupied orbitals of opposite spin are located at higher energies, one of which results in the unoccupied level located just below the conduction band [Fig. 3(c)]. The projections of the unoccupied states on the atomic orbitals situate the unoccupied p orbital corresponding to the higher occupied level in the band gap at ∼0.15 eV above the conduction band. This state is only partially localized on one carbon atom of the C–C pair due to its resonance with the conduction states of SiC. The modeling of the carbon interstitial in bulk 4H-SiC indicates that trap states related to carbon defects in the substrate can be present

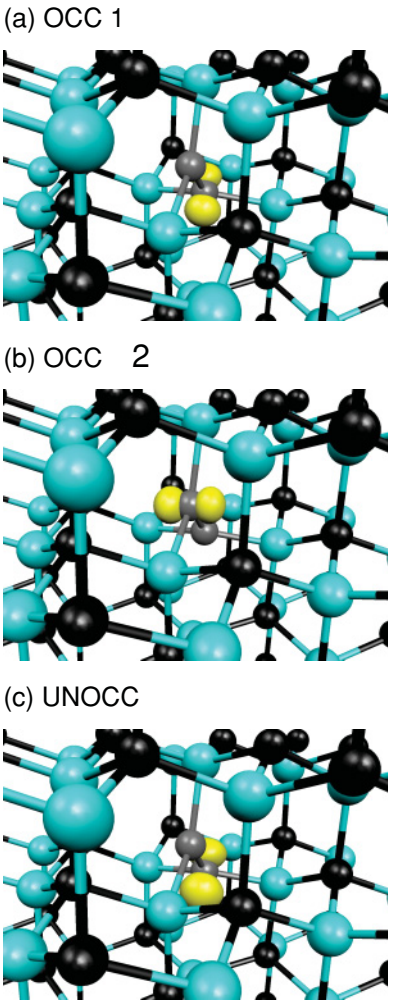

FIG. 3. (Color online) Isosurfaces of the density (0.15 a.u.) of the C–C pair-related defect states in the 4H-SiC band gap, as identified in Fig. 2.

in the upper part of the band gap, in contrast with previous studies.[12,14]

To evaluate the effects of structural relaxation upon charging, we also derive charge transition levels associated with the charging of the first unoccupied defect state of the carbon interstitial in bulk SiC. Adopting the PBE(0.15) hybrid functional, we obtained the $0/-$ charge transition level from the difference between the total energies of the neutral and the negatively charged state.[25] We account for finite-size effects by considering the first-order Makov-Payne correction[26] and the shift ΔV of the average potential.[25] We first considered the vertical charge transition level, which is obtained without considering any structural relaxation in the charged state. The level is found at 3.11 eV from the valence band maximum, in close correspondence with the Kohn-Sham level at 3.10 eV [cf. Fig. 2(b)]. When a full structural relaxation of the negatively charged defect state is carried out, the $0/-$ charge transition level drops to 2.52 eV. This result corroborates our finding that the trapping of an electron indeed leads to a defect state within the SiC band gap. From the quantitive point of view, the present result indicates that the consideration of the structural relaxation in the charged state might lead to an appreciable shift of 0.6 eV to lower energies for this kind of defects.

B. Carbon pairs in SiC at the 4H-SiC/SiO_2 interface

Adopting the model of the 4H-SiC/SiO_2 interface introduced in Sec. II, we here study the carbon pair defect in five different configurations on the substrate side of the SiC/SiO_2 interface. Ball-and-stick representations of the considered configurations are displayed in Fig. 4.

In configurations Si_2–C–C–Si_2 and $(Si_2–C–C–Si_2)'$, a carbon interstitial shares a carbon lattice site with an atom of the SiC substrate. These two configurations only differ by the

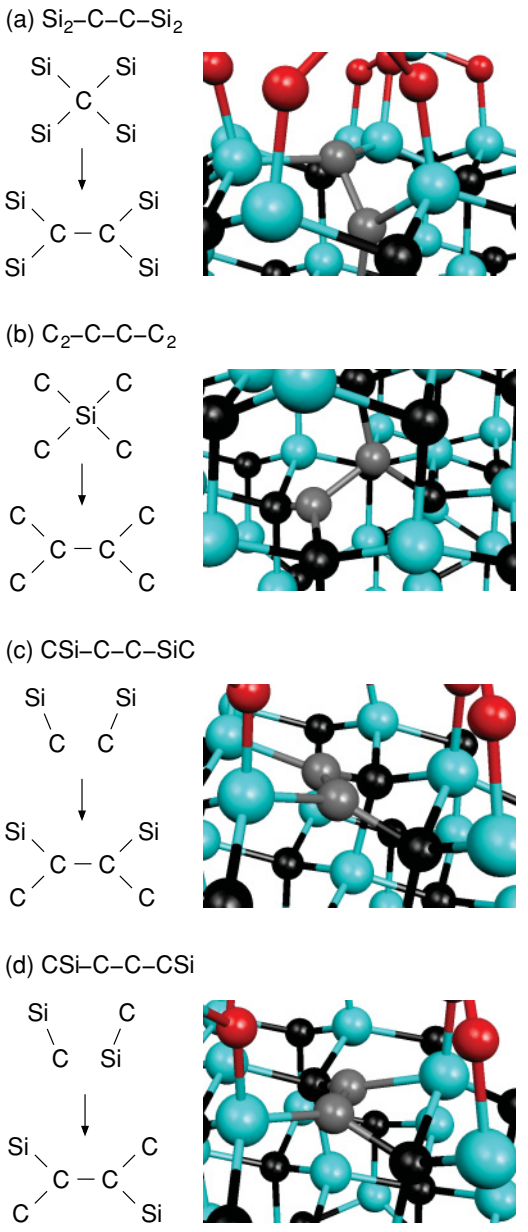

FIG. 4. (Color online) (a)–(d) The carbon pair defect in SiC at the SiC/SiO_2 interface in four different configurations. A variant of the configuration in (a) is also modeled and labeled as $(Si_2–C–C–Si_2)'$ (see text).

TABLE I. Distance and angle parameters of the X_2–C–C–X_2 structures (X refers to Si or C) in the SiC substrate. The structures are labeled according to Fig. 4. In the case of the last two structures, C–C and then Si–C distances are given in the corresponding column. Distances are given in Å. The last two columns give the angle between the planes of the two sp^2 hybridized carbon atoms and the average dihedral angles of the X_2–C–C–X_2 structure, respectively. Standard deviations are given in parentheses.

	C–C	X–C	$\angle$ X–C–X	$\angle(sp^2$ pl.)	$\sigma_{\angle\ \mathrm{dih.}}$
Si_2–C–C–Si_2	1.39	1.80	134.9° (4.2°)	89.7°	74.9° (2.3°)
$(Si_2$–C–C–$Si_2)'$	1.38	1.79	138.2° (0.9°)	89.5°	89.0° (0.7°)
C_2–C–C–C_2	1.43	1.54	137.5° (1.5°)	89.4°	82.4° (0.8°)
CSi–C–C–SiC	1.37	1.46/1.78	121.3° (1.0°)	15.3°	49.6° (3.5°)
CSi–C–C–CSi	1.38	1.45/1.75	127.1° (10.0°)	38.1°	52.5° (7.2°)

position of the defect with respect to the plane of the interface, and thus only configuration Si_2–C–C–Si_2 is represented in Fig. 4(a). In this configuration, the carbon lattice site locates in the last C plane of the SiC substrate, thereby placing the C–C pair in the immediate vicinity of the interface. In configuration $(Si_2$–C–C–$Si_2)'$, the C–C pair is situated farther down into the substrate, at about 3 Å from the interface. The third considered configuration is C_2–C–C–C_2 [Fig 4(b)]. Here the carbon pair replaces a Si atom in the last-by-one Si plane of the SiC substrate. Each carbon atom of the pair therefore bonds to two other carbon atoms as opposed to silicon atoms in the first two configurations. The fourth and fifth configurations are obtained by the insertion of a C–C pair into the substrate [Figs. 4(c) and 4(d)]. This gives rise to intermediate situations in which each carbon atom of the interstitial C–C pair bonds to one silicon atom and one carbon atom of the substrate. The difference between the last two configurations comes from the relative positions of the silicon atoms bonding to the carbon atoms of the C–C pair. When looking along the C–C bond, the two silicon atoms can either be found on the same side, as for CSi–C–C–SiC in Fig. 4(c), or on opposite sides as, for CSi–C–C–CSi in Fig. 4(d). The main structural parameters of the relaxed defect models are summarized in Table I.

In Sec. III A, it was shown that the defect levels associated with the carbon pair originate from nonbonding p orbitals of the carbon atoms when the planes of their sp^2 hybridized orbitals are nearly perpendicular. The first three configurations, that is, Si_2–C–C–Si_2 [Fig. 4(a)], $(Si_2$–C–C–$Si_2)'$, and C_2–C–C–C_2 [Fig. 4(b)], share this feature. The defect configurations Si_2–C–C–Si_2 and $(Si_2$–C–C–$Si_2)'$ only differ by their distance from the interface, only the former being represented in Fig. 4(a). Their distance and angle parameters are rather similar and the overall defect configuration remains unchanged. Nevertheless, when compared to the analogous bulk defect (cf. Sec. III A), the Si_2–C–C–Si_2 configuration lying closer to the interface [Fig. 4(a)] is found to undergo slightly larger structural rearrangements. In the C_2–C–C–C_2 defect model [Fig. 4(b)], the distances between carbon atoms of the C–C pair and their neighbors are strongly reduced, leaving more space for the C–C pair than in the previous configurations. However, despite the different chemical nature of the neighbors of the paired carbon atoms, the overall structure remains very similar to the first two defect configurations. In the last two configurations, CSi–C–C–SiC [Fig. 4(c)] and CSi–C–C–CSi [Fig. 4(d)], a carbon pair interstitial is introduced in the close vicinity of the interface. The addition of two carbon atoms in the last planes of the substrate results in a contraction of the bond lengths between the carbon atoms of the C–C pair and their neighbors compared to the first three structures. However, the main difference resides in the angle between the planes of the two sp^2 hybridized carbon atoms. Whereas the planes of the two sp^2 hybridized carbon atoms are nearly perpendicular in the first three structures [Figs. 4(a) and 4(b)], they are almost parallel in the last two configurations [Fig. 4(c) and 4(d)].

We then turn to the electronic configurations of these defect structures at the interface. Due to the quantum confinement effects related to the finite thickness of the substrate, the SiC band edges determined from the local density of states are biased. Hence, the defect levels are aligned to the bulk band extrema through the local electrostatic potential. Figure 5 shows the defect levels associated with the carbon pair calculated at the PBE and PBE(0.15) levels of theory.[27] The quantum confinement of the substrate in the interface structure induces a band gap opening of SiC (cf. Sec. II). In the interface structure, some well-localized defect levels close to the band extrema but in the band gap of SiC, as found in the interface model, can therefore appear above the conduction band inferred from the alignment of the bulk band structure.

Overall, the electronic structures of the defects as obtained with the two functionals agree very well. In particular, occupied levels aligned with respect to the valence band do not differ by more than 0.03 eV. Similarly, the unoccupied levels show differences of at most a few tenths of an eV when referred to the conduction band edge.

The electronic structures of the defects Si_2–C–C–Si_2 [Fig. 4(a)], $(Si_2$–C–C–$Si_2)'$, and C_2–C–C–C_2 [Fig. 4(b)] appear very similar. In all these configurations, two occupied levels locate between about 0.7 and 1.2 eV above the valence band and their separation ranges from 0.1 to 0.3 eV (Fig. 5). Contrarily to previous studies,[12,14] we also found unoccupied levels within the SiC band gap. Two unoccupied levels lie between 0.4 eV below the conduction band and 0.2 eV above the conduction band and are 0.1 to 0.5 eV apart (Fig. 5). The observed differences in energy position can be attributed to the local environment of the defect C–C pair. In particular, when a carbon atom shares a carbon lattice site, the location of the first unoccupied level in the SiC band gap can vary by 0.4 eV depending on whether the defect structure is located in the vicinity of the interface [cf. Si_2–C–C–Si_2, Fig. 4(a)] or farther down in the substrate [cf. $(Si_2$–C–C–$Si_2)'$], due to different structural relaxations. In a perfectly symmetric arrangement around the C–C pair and provided their interaction can be neglected, the two occupied and the

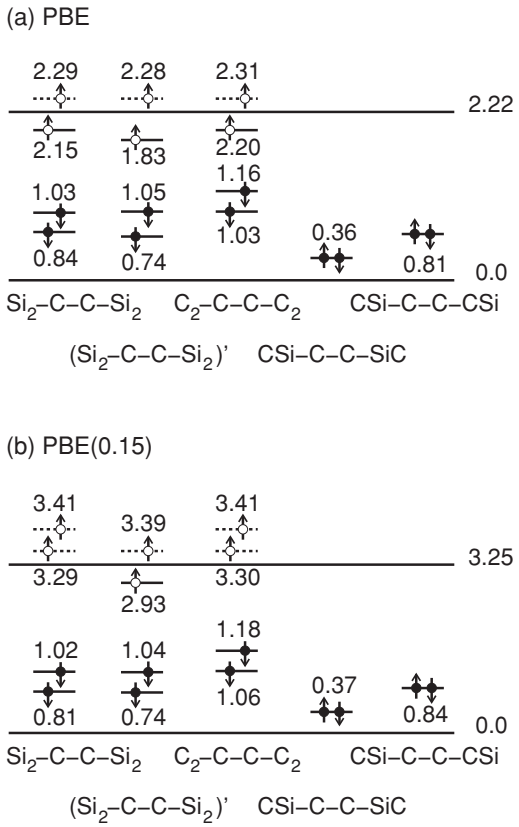

FIG. 5. (a) PBE and (b) PBE(0.15) defect levels related to the carbon pair defect in SiC at the SiC/SiO_2 interface in the five configurations considered (cf. Fig. 4). The majority and minority spin electrons are denoted by downward and upward arrows, respectively, and the occupied and unoccupied levels are represented by solid and open circles, respectively. The unoccupied levels located above the SiC conduction band are represented by dotted lines. Energies are given in eV.

two unoccupied carbon levels would be degenerate and located at the same energy. Depending on the structural relaxations allowed by the local constraints of the environment, departures from this ideal situation occur and the two occupied and the two unoccupied levels split. Despite these small differences in energy levels, the occupied and unoccupied levels in all three defect configurations share the same origin.

In defect structures CSi–C–C–SiC [Fig. 4(c)] and CSi–C–C–CSi [Fig. 4(d)], a different situation occurs. In contrast with the first three defect structures, the angle between the planes of the two sp^2 hybridized carbon atoms is far from 90°. In these cases, the p orbitals of the carbon atoms of the C–C pair can overlap and form a π bond. The isosurface of the occupied defect state associated to the carbon pair in the CSi–C–C–SiC structure is shown in Fig. 6(a). This results in a defect level doubly occupied in the lower part of the SiC band gap. As noticed for the unoccupied levels in the first three structures, the different local environments (in particular the angle between the planes of the two sp^2 hybridized carbon atoms in this case) account for the variation of the defect level position. The corresponding unoccupied level does not occur in the band gap.

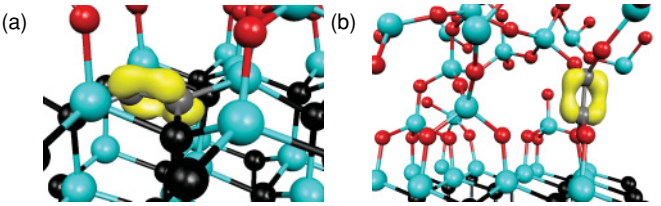

FIG. 6. (Color online) Isosurface of the density (0.15 a.u.) of the occupied defect state related to the carbon pair in the (a) CSi–C–C–SiC and (b) O_2–C–C–O_2 structures.

C. Carbon pairs in SiO_2 at the 4H-SiC/SiO_2 interface

During the SiC oxidation, carbon atoms could incorporate in the SiO_2 oxide. We therefore investigate possible configurations of the C–C pair in the oxide. In the considered series, the carbon atoms bond to each other and to either (i) one silicon atom and one oxygen atom [SiO–C–C–SiO; Fig. 7(a)], (ii) two oxygen atoms [O_2–C–C–O_2; Fig. 7(b)], or (iii) two silicon atoms [Si_2–C–C–Si_2; Fig. 7(c)]. For every kind of bonding, we consider two variants, the second one being denoted by a prime.

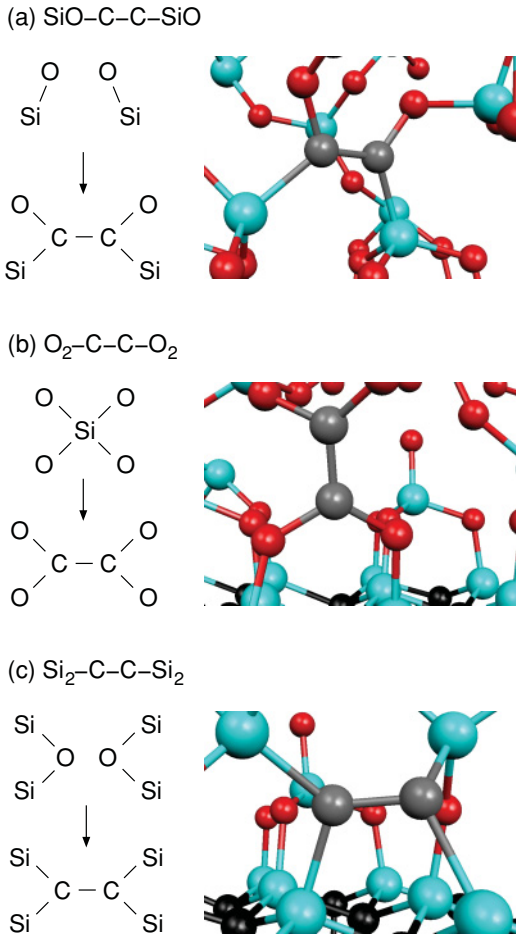

FIG. 7. (Color online) The carbon pair defect in SiO_2 at the SiC/SiO_2 interface in three representative configurations. The insertion of the C–C pair in various environments is represented schematically and the corresponding ball-and-stick representations of the relaxed structures are shown.

TABLE II. Distance and angle parameters of the X_2–C–C–X_2 structures (X refers to Si or C) in the oxide. The structures are labeled according to Fig. 7. Distances are given in Å. The last two columns give the angle between the planes of the two sp^2 hybridized carbon atoms and the average dihedral angle of the X_2–C–C–X_2 structure, respectively. Standard deviations are given in parentheses.

	C–C	O–C	Si–C	$\angle$ X–C–X	$\angle(sp^2$ pl.)	$\sigma_{\angle}$ dih.
SiO–C–C–SiO	1.36	1.38	1.87	118.0° (6.6°)	10.1°	11.1° (8.1°)
(SiO–C–C–SiO)′	1.39	1.39	1.87	128.9° (1.1°)	31.9°	10.4° (6.1°)
O_2–C–C–O_2	1.36	1.37	–	117.8° (2.1°)	16.3°	16.2° (0.9°)
(O_2–C–C–O_2)′	1.35	1.37	–	119.1° (0.9°)	51.0°	72.5° (4.3°)
Si_2–C–C–Si_2	1.38	–	1.91	118.0° (3.9°)	48.5°	51.0° (23.5°)
(Si_2–C–C–Si_2)′	1.40	–	1.92	100.0° (2.9°)	53.3°	52.3° (5.7°)

For the construction of the SiO–C–C–SiO defect, we inserted two carbon atoms at the interface by disrupting Si–O bonds [Fig. 7(a)]. In the first variant, the Si–O bonds that the C–C pair disrupts involve silicon atoms of the first Si plane of the oxide and oxygen atoms of the second O plane. The second variant involves silicon atoms of the terminating Si plane of the substrate. We constructed the O_2–C–C–O_2 defect model by replacing a silicon atom belonging to the first Si plane of the oxide with a C–C pair [Fig. 7(b)]. The two variants differ by the choice of the replaced silicon atom. For achieving Si_2–C–C–Si_2 defects, we replaced two neighboring oxygen atoms with a C–C pair [Fig. 7(c)]. In the first variant, the replaced oxygen atoms belong to the first O plane of the oxide, whereas in the second one the C–C pair is located at about 12 Å from the interface.

Table II summarizes the bond lengths and bond angles of the defect structures. The distance between the carbon atoms of the C–C pair and the distance between carbon atoms of the C–C pair and oxygen/silicon neighbors are very similar in the six defect structures. In contrast, the angle parameters cover a wide range of values. In particular, the angle between the planes of the two sp^2 hybridized carbon atoms varies between 10° and 53°, at variance with the C–C pair defect structures in SiC. The standard deviation of the dihedral angles involving the C–C pair also describes the large departure from the modeling of the C–C pair in SiC where the defect structure could be schematically represented as two orthogonal planes with all dihedral angles close to 90°. The amorphous SiO_2 network is indeed more deformable than the SiC crystal and can accomodate more easily important structural relaxations.

Figure 8 shows the defect levels of the six C–C pair defect configurations calculated at the PBE and PBE(0.15) levels of theory. The descriptions of the occupied and unoccupied levels correspond very well and their locations with respect to the valence band and conduction band agree within 0.1 eV. In all six defect structures a doubly occupied level locates in the low/mid part of the band gap. In contrast with the first three defect structures modeled in the SiC substrate, the angle between the two planes formed by each carbon atom of the C–C pair and its neighbors is far from 90° and varies between 10° and 53°. In these cases, the p orbitals of the carbon atoms of the C–C pair can overlap and form a π bond as in the last two defect configurations modeled in SiC at the interface. The isosurface of the occupied defect state related to the carbon pair in the O_2–C–C–O_2 structure is very similar to that of the CSi–C–C–SiC structure modeled in SiC and is shown in Fig. 6(b).

For each bonding configuration, the two considered variants sample different structural representation of the C–C pair defect with the same neighboring environment. Despite their different structural parameters, in particular, the angle between the planes of the sp^2 hydridized carbon atoms, the occupied defect levels remain almost unchanged for a given shell of nearest neighbors. Hence, the angle between the planes of the sp^2 hydridized carbon atoms appears critical to determine whether one finds two singly occupied unpaired orbitals or one doubly occupied paired orbital. However, within the range of angles allowing for π bonding, the energy level does not appear to depend in a perceptible way on this angle.

Another difference with the models of the C–C pair defect in SiC can be seen in the detection of unoccupied levels.

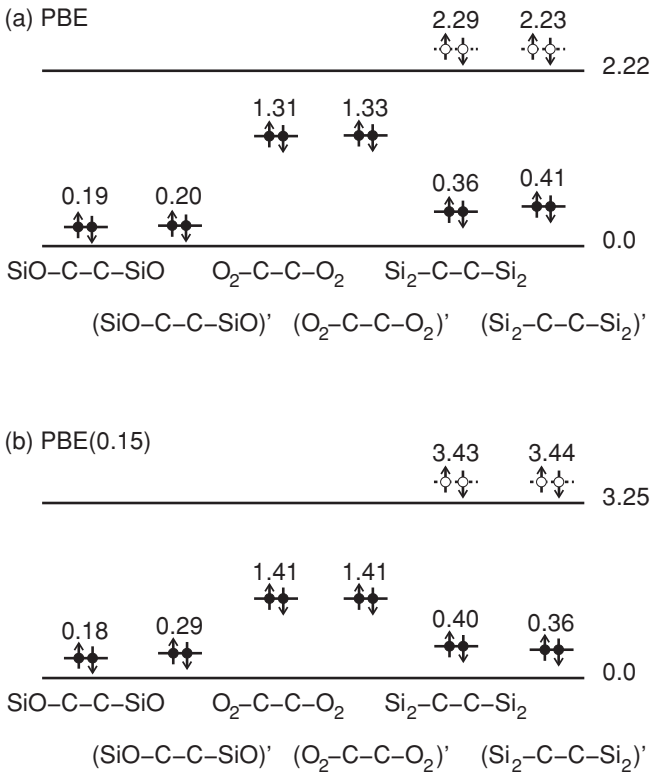

FIG. 8. Defect levels related to the carbon pair defect in various configurations (cf. Fig. 7). The occupied and unocuppied levels are represented by solid and open circles, respectively. Unoccupied levels located above the SiC conduction band are represented by dotted lines. Energies are given in eV.

The antibonding π orbital could be detected only in the configuration where the C–C pair bonds to four Si atoms [Fig. 7(c)], as studied earlier by Knaup *et al.*[13] In the two variants of the Si_2–C–C–Si_2 defect, our calculations locate the unoccupied states slightly above the conduction band of SiC, independent of distance of the defect to the interface. Knaup *et al.* located this level just below the conduction band,[13] but such small variations could depend on different structural details. It can therefore not be ruled out that the defect levels of some C–C pair defect in the near interface oxide appears below the SiC conduction band. However, a more significant difference of our results with respect to those of Knaup *et al.* concerns the location of the highest occupied level of the Si_2–C–C–Si_2 defect. In our calculation, it is found well within the SiC band gap establishing thereby a clear correlation with the appearance of an unoccupied state in the vicinity of the conduction band. At variance, Knaup *et al.* found this level to lie below the valence band maximum.[13]

D. Investigation of the C–C pair defect via molecular models

We have modeled C–C pair defects in the SiC substrate and in SiO_2. In both cases, defect states located around the conduction band of SiC could be identified. To investigate the energy range that these defect states can span, we here study the C–C pair via molecular models. The variety of possible bonding environments of the C–C pair and the complex structural arrangements lead to a distribution of defect levels. However, a major parameter appears to be the relative orientation of the p orbitals of the two sp^2 hybridized carbon atoms. We therefore investigate the positions of the defect levels of the C–C pair versus the angle between the planes of the two sp^2 hybridized carbon atoms. We study three molecules in which the C–C pairs show the same neighbors as in the defect structures at the interface: $C_2(SiH_3)_4$, $C_2(CH_3)_4$, and $C_2(OH)_4$. The geometry of the molecules is fully relaxed with the only constraint being the angle between the planes of the two sp^2 hybridized carbon atoms which is kept fixed at angles varying between 0° and 90°. Figure 9 shows the isosurfaces of the density of the C–C states in the $C_2(SiH_3)_4$ molecule when the angle between the planes of the two sp^2 hybridized carbons is 0°, 45°, and 90°. The two angles 0° and 90° lead to isosurfaces very similar to the ones of the C–C defect structures in SiO_2, where the p orbitals are nearly parallel and pair up, and in SiC, where the p orbitals are almost perpendicular and do not overlap, respectively. The positions of the highest occupied and lowest unoccupied defect levels of the C–C pair vs the angle between the planes of the two sp^2 hybridized carbons are shown in Fig. 10 for the $C_2(SiH_3)_4$ molecule. The other molecules show a very similar behavior. The main characteristic energies defined in Fig. 10 are reported in Table III for all three molecules.

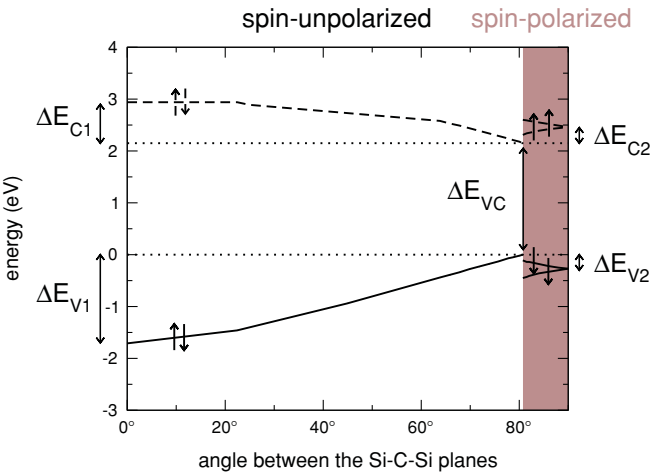

FIG. 10. (Color online) Evolution of the highest occupied level(s) and lowest unoccupied level(s) in the $C_2(SiH_3)_4$ molecule for the angle between the planes of the two sp^2 hybridized carbon atoms varying between 0° and 90°. The energies are referred to the highest occupied level. The same trends are found for the $C_2(CH_3)_4$ and $C_2(OH)_4$ molecules. The values of the characteristic energies indicated are given in Table III.

In all three molecules, the smallest separation between the highest occupied and lowest unoccupied levels occurs when the most stable configuration switches from a spin-unpolarized to a spin-polarized configuration around 80°. The largest separation between occupied and unoccupied levels is obtained when the planes of the two sp^2 hybridized carbon atoms are parallel. When they are orthogonal, the highest occupied level and the lowest unoccupied level are shifted down and up by about 0.3–0.8 eV with respect to their maximum and minimum value, respectively (cf. Table III).

The picture provided by these molecular models is partial as the only parameter is the angle between the planes of the two sp^2 hybridized carbon atoms. However, it highlights some interesting features of the C–C pair defect. First, the defect

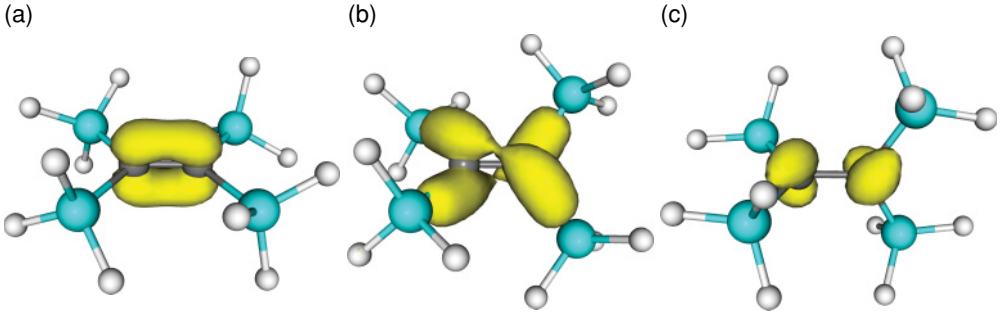

FIG. 9. (Color online) Isosurface of the density (0.15 a.u.) of the p orbitals in the $C_2(SiH_3)_4$ molecule when the angle between the planes of the two sp^2 hybridized carbon atoms is (a) 0°, (b) 45°, and (c) 90°.

TABLE III. Characteristic energy values (in eV) describing the evolution of the highest occupied and lowest unoccupied levels as a function of the angle between the planes of the two sp^2 hybridized carbon atoms in the $C_2(SiH_3)_4$, $C_2(CH_3)_4$, and $C_2(OH)_4$ molecules, as obtained at the PBE(0.15) level of theory. The energies are defined in Fig. 10.

	ΔE_{VC}	ΔE_{V1}	ΔE_{V2}	ΔE_{C1}	ΔE_{C2}
$C_2(SiH_3)_4$	2.2	1.7	0.3	0.8	0.3
$C_2(CH_3)_4$	2.5	1.8	0.4	1.9	0.7
$C_2(OH)_4$	2.6	0.9	0.4	2.8	0.8

states of the C–C pair near the SiC conduction band that have lower energies can be identified and occur for an angle between the planes of the two sp^2 hybridized carbon atoms close to ∼80°. This situation occurs much more frequently in the SiC substrate where the tetrahedra formed by the atoms bonded to the C–C pair cannot be strongly distorted. On the other hand, the structure around a C–C pair in amorphous SiO_2 can relax much more easily and accomodate a π bond stabilizing the system. This accounts for the rare detection of unoccupied C–C levels when the defect is modeled in SiO_2 in contrast with the modeling in SiC. Second, the chemical nature of the atoms bonded to the C–C pair has an impact on the splitting between occupied and unoccupied levels. The $C_2(SiH_3)_4$ molecules features the smallest separation between occupied and unoccupied levels throughout the whole angle range. The only unoccupied levels detected in the six defect models in the oxide are indeed associated with Si_2–C–C–Si_2 structures. In the SiC substrate, the lowest unoccupied C–C level detected also derives from the Si_2–C–C–Si_2 defect structure.

The qualitative comparison between the separations of the occupied and unoccupied levels of the Si_2–C–C–Si_2 structures at the interface and of the $C_2(SiH_3)_4$ molecule is also instructive. The Si_2–C–C–Si_2 structure embedded in SiO_2 [Fig. 7(c)] features a level separation of 3.0 eV at the PBE(0.15) level of theory. When the angle between the planes of the two sp^2 hybridized carbon atoms of the $C_2(SiH_3)_4$ molecule has the same value of ∼49°, the level separation is 3.6 eV, in reasonable agreement with the value for the defect structure in SiO_2. When an analogous comparison for the two Si_2–C–C–Si_2 structures in SiC [Fig. 4(a)] is performed, a similar agreement is obtained with an average level separation of 2.1 eV for the interface structures, to be compared with a level separation of 2.7 eV for the molecule with an angle of 90°. This agreement is sufficiently good to use the molecular models together with the modeled defect structures at the interface for an estimation of the energy range of the C–C defect levels. Combining these two approaches allows us to consider, on the one hand, all the possible angles between the planes of the two sp^2 hybridized carbon atoms, and, on the other hand, the effect of the interfacial environment. Taking $E^{mol}_{90°}$ as the energy of the lowest unoccupied level in the $C_2(SiH_3)_4$ molecule when the angle between the planes of the two sp^2 hybridized carbon atoms is 90°, we note from Fig. 10 that the minimum of the lowest unoccupied level in the $C_2(SiH_3)_4$ molecule locates at $E^{mol}_{90°} - 0.3$ eV, when the angle between the planes of the two sp^2 hybridized carbon atoms is 78°. As the modeled Si_2–C–C–Si_2 structures in SiC at the interface [Fig. 4(a)] also feature an angle ∼90°, we can align the average energy of the lowest unoccupied level in the modeled Si_2–C–C–Si_2 structure in SiC to $E^{mol}_{90°}$ of the $C_2(SiH_3)_4$ molecule. Finally, this gives a minimum value for the lowest unoccupied level at the interface located at about 0.4 eV below the SiC conduction band. This suggests that this type of defect gives rise to a rather broad distribution of energy levels.

E. Single carbon atoms in SiO_2 at the 4H-SiC/SiO_2 interface

Two defect structures involving single carbon atoms on the oxide side of the SiC/SiO_2 interface are studied here. We first consider a carbon atom replacing a silicon atom and forming a bond to four oxygen atoms of the oxide. Then we study a carbon atom replacing an oxygen atom in a Si–O–Si bond and thus forming a Si_2–C–O structure. Ball-and-stick representations of these two configurations are shown in Figs. 11(a) and 11(b).

When one carbon atom replaces one silicon atom in the oxide network [Fig. 11(a)], the structural rearrangement is driven by the shorter C–O distance. In the relaxed structure, the average C–O bond length is 1.41 Å, about 16% shorter than the average Si–O bond length in the oxide. All the other structural parameters remain almost unchanged upon replacement of a silicon atom by a carbon atom. In the Si_2–C–O structure [Fig. 11(b)], the carbon atom is threefold coordinated. The angle between the two planes defined by the Si–C–O atoms is only 11.2°, making the overall structure almost planar. The Si–C bond lengths of 1.87 Å are comparable to the bond length in the SiC substrate, and the C–O bond length is 1.23 Å. The Si–C–O angles are about 122°.

The electronic structure of the configuration in which a carbon atom replaces a Si atom [Fig. 11(a)] does not reveal any defect level in the SiC band gap. The chemical similarity of

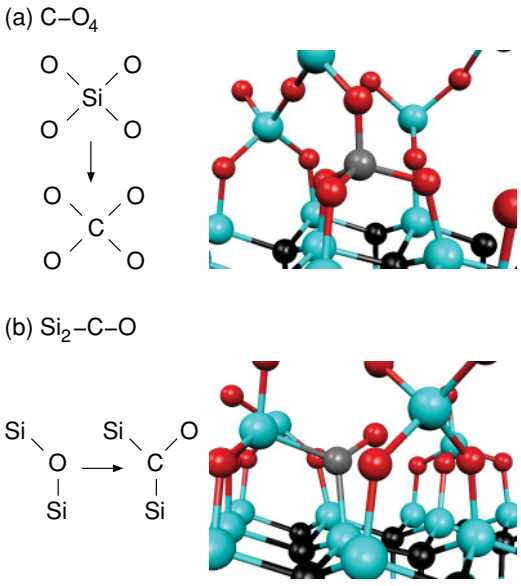

FIG. 11. (Color online) Schematic and ball-and-stick representations of the (a) C–O_4 and (b) Si_2–C–O structures.

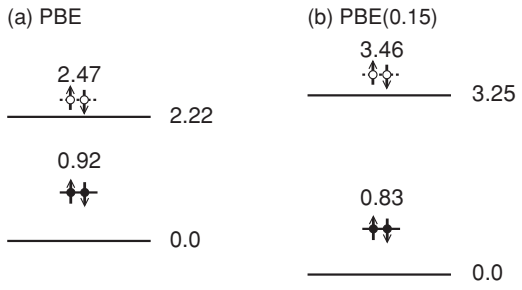

FIG. 12. Defect levels associated with the carbon atom of the Si_2–C–O structure shown in Fig. 11(b). The occupied and unocuppied levels are represented by solid and open circles, respectively. Unoccupied levels located above the SiC conduction band are represented by dotted lines.

carbon and silicon accounts for this. In the Si_2–C–O structure [Fig. 11(b)], one doubly occupied defect level lies in the lower part of the SiC band gap as found previously by Wang *et al.*,[14] while one unoccupied level locates slightly above the SiC conduction band (see Fig. 12). These defect levels can be attributed to one of the oxygen lone pairs and to the π^* antibonding orbital, respectively (Fig. 13). The second oxygen lone pair is lower in energy and does not give any level in the gap. The overall picture for the unoccupied defect level is very similar to that of the C–C pair when the planes of the two sp^2 hybridized carbons are nearly parallel.

IV. CONCLUSIONS

We investigated candidate carbon single-atom and pair defects at the SiC/SiO_2 interface with the aim of determining their contribution to the D_{it} in the SiC band gap. We resorted to a scheme based on hybrid density functionals in order to overcome the band gap underestimation of semilocal functionals, which would prevent an unambiguous comparison between theory and experiment. Indeed, the identification of typical near interface defects is expected to mainly rest on the position of energy levels with respect to the relevant band edges.

Since the carbon interstitial in SiC gives rise to a defect structure involving a pair of carbon atoms, we focused on a variety of such carbon pair defects in various locations across the SiC/SiO_2 interface. The C–C pair defect involving sp^2 hybridized carbon atoms in bulk SiC was found to give occupied defect energy levels in the low/mid part of the SiC band gap but also unoccupied levels in the upper part of the SiC band gap. The electronic defect levels of various C–C pairs configurations on the substrate and oxide sides of the SiC/SiO_2 interface were then investigated. Despite their structural differences, their energy levels showed a similar pattern as in bulk SiC. The study of the C–C pair defect via molecular models showed that the positions of its defect levels in the SiC band gap depend on the chemical nature of the neighbors of the C–C pair and on the relative orientation of the planes of the two sp^2 hybridized carbon atoms.

Our study also comprised two carbon single-atom defects on the oxide side of the SiC/SiO_2 interface. When the carbon atom is substitutional to a Si atom, no defect levels were found in the SiC band gap. The other carbon single-atom defect concerned a carbon atom incorporating at an oxygen site and giving rise to a Si_2–C–O structure. This defect shows an occupied defect level in the lower part of the SiC band gap and an unoccupied defect level close to the SiC conduction band, in close analogy to the carbon pair defects.

These results indicate that defects involving just one or two carbon atoms concurrently contribute to the defect density in the low/mid part of the SiC band gap and near the SiC conduction band, establishing a strong correlation between the defect densities in these energy ranges. Our study shows that the contribution of these carbon defects to the defect density is expected to consist of broad peaks because of the sensitivity to the local structure and environment. Therefore, it is reasonable to assume that such defects contribute to the background level of the defect density in large portions of the SiC band gap. However, inspection of the experimental defect density at the SiC/SiO_2 interface also reveals the occurrence of an intense and narrow peak in the vicinity of the SiC conduction band. This peak does not appear to correlate with any significant defect density in the lower part of the SiC band gap. Hence, these considerations suggest that the dominant contribution to the peak occurring in the vicinity of the SiC conduction band cannot originate from the carbon defects studied in this work. The origin of the experimentally detected near-interface trap levels could thus not be identified and remains elusive.

In the present study, we scrutinized various candidate defects via their Kohn-Sham energy levels providing a picture based on chemical intuition and molecular orbitals, toward the identification of the main contributors to the defect density of states at the SiC/SiO_2 interface. From our study, it also appears that the consideration of structural relaxation upon defect charging could lead to an improved quantitative description of the defect levels.

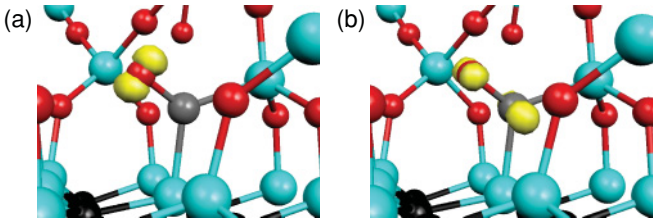

FIG. 13. (Color online) Isosurface of the density (0.15 a.u.) of (a) the occupied and (b) the unoccupied defect state in the Si_2–C–O structure, as identified in Fig. 12.

ACKNOWLEDGMENTS

We acknowledge useful interactions with V. V. Afanas'ev, P. Deák, S. Dhar, L. C. Feldman, E. L. Garfunkel, and H. Ö. Ólafsson. Partial support from the Swiss National Science Foundation is acknowledged (Grant No. 200020-111747). Most of the calculations were performed on the BlueGene computer of EPFL. We also used the cluster PLEIADES-EPFL and other computational facilities at DIT-EPFL, CSEA-EPFL, and CSCS.

[1]V. V. Afanas'ev, A. Stesmans, M. Bassler, G. Pensl, M. J. Schulz, and C. I. Harris, Appl. Phys. Lett. **68**, 2141 (1996).
[2]V. V. Afanasev, M. Bassler, G. Pensl, and M. J. Schulz, Phys. Status Solidi A **162**, 321 (1997).
[3]V. V. Afanas'ev, F. Ciobanu, S. Dimitrijev, G. Pensl, and A. Stesmans, J. Phys. Condens. Matter **16**, S1839 (2004).
[4]V. V. Afanas'ev, M. Bassler, G. Pensl, and M. J. Schulz, J. Appl. Phys. **79**, 3108 (1996).
[5]C. Virojanadara and L. I. Johansson, Surf. Sci. Lett. **472**, L145 (2001).
[6]C. Virojanadara and L. I. Johansson, Surf. Sci. **505**, 358 (2002).
[7]J. L. Cantin, H. J. von Bardeleben, Y. Shishkin, Y. Ke, R. P. Devaty, and W. J. Choyke, Phys. Rev. Lett. **92**, 015502 (2004).
[8]J. L. Cantin, H. J. von Bardeleben, Y. Ke, R. P. Devaty, and W. J. Choyke, Appl. Phys. Lett. **88**, 092108 (2006).
[9]S. Dhar, L. C. Feldman, S. Wang, T. Isaacs-Smith, and J. R. Williams, J. Appl. Phys. **98**, 014902 (2005); S. Dhar, S. Wang, A. C. Ahyi, T. Isaacs-Smith, S. T. Pantelides, J. R. Williams, and L. C. Feldman, Mater. Sci. Forum **527–529**, 949 (2006).
[10]S. T. Pantelides, S. Wang, A. Francesschetti, R. Buczko, M. Di Ventra, S. N. Rashkeev, L. Tsetseris, M. H. Evans, I. G. Batyrev, L. C. Feldman, S. Dhar, K. McDonald, R. A. Weller, R. D. Scrimpf, D. M. Fleetwood, X. J. Zhou, J. R. Williams, C. C. Tin, G. Y. Chung, T. Isaacs-Smith, S. R. Wang, S. J. Pennycook, G. Duscher, K. van Benthem, and L. M. Porter, Mater. Sci. Forum **527–529**, 935 (2006).
[11]P. Deák, J. M. Knaup, T. Hornos, C. Thill, A. Gali, and T. Frauenheim, J. Phys. D: Appl. Phys. **40**, 6242 (2007).
[12]J. M. Knaup, P. Deák, Th. Frauenheim, A. Gali, Z. Hajnal, and W. J. Choyke, Phys. Rev. B **71**, 235321 (2005).
[13]J. M. Knaup, P. Deák, Th. Frauenheim, A. Gali, Z. Hajnal, and W. J. Choyke, Phys. Rev. B **72**, 115323 (2005).
[14]S. Wang, S. Dhar, S. R. Wang, A. C. Ahyi, A. Franceschetti, J. R. Williams, L. C. Feldman, and S. T. Pantelides, Phys. Rev. Lett. **98**, 026101 (2007).
[15]F. Devynck, F. Giustino, P. Broqvist, and A. Pasquarello, Phys. Rev. B **76**, 075351 (2007).
[16]J. P. Perdew, M. Ernzerhof, and K. Burke, J. Chem. Phys. **105**, 9982 (1996).
[17]J. P. Perdew, K. Burke, and M. Ernzerhof, Phys. Rev. Lett. **77**, 3865 (1996).
[18]N. Troullier and J. L. Martins, Phys. Rev. B **43**, 1993 (1991).
[19]A. Alkauskas, P. Broqvist, F. Devynck, and A. Pasquarello, Phys. Rev. Lett. **101**, 106802 (2008).
[20]P. Broqvist, A. Alkauskas, and A. Pasquarello, Phys. Rev. B **80**, 085114 (2009); **81**, 039903(E) (2010).
[21]CPMD v3.11.1, copyright IBM Corp 1990–2006, copyright MPI für Festkörperforschung Stuttgart 1997–2001; J. Hutter and A. Curioni, Chem. Phys. Chem. **6**, 1788 (2005).
[22]Yoon Soo Park, in *SiC Materials and Devices*, edited by R. K. Willardson and E. R. Weber (Academic Press, San Diego, 1998).
[23]P. Broqvist and A. Pasquarello, Microelectron. Eng. **84**, 2022 (2007).
[24]P. Deák, B. Aradi, T. Frauenheim, E. Janzén, and A. Gali, Phys. Rev. B **81**, 153203 (2010).
[25]C. G. Van de Walle and J. Neugebauer, J. Appl. Phys. **95**, 3851 (2004).
[26]G. Makov and M. C. Payne, Phys. Rev. B **51**, 4014 (1995).
[27]To assess the convergence of the defect levels with the finite thickness of the SiC slab, calculations at the PBE level were carried out with the thickness of SiC doubled. The positions of the defect levels did not shift by more than 0.1 eV.